The AP-1 complex regulates AXL expression and determines sensitivity to PI3Kα inhibition in esophagus and head and neck squamous cell carcinoma

Mai Bdarny*[1,2], Manu Prasad*[1,2], Noa Balaban[1,2], Joshua Ben-Zion[2,3], Anat Bahat Dinur[2,3], Reidar Grénman[4], Limor Cohen*[#1,2], Moshe Elkabets[#1,2]

Affiliations:

1. The Shraga Segal Department of Microbiology, Immunology and Genetics, Ben-Gurion University of the Negev, Beer-Sheva 84105, Israel
2. Faculty of Health Sciences, Ben-Gurion University of the Negev, Beer-Sheva 84105, Israel
3. Department of Otolaryngology-Head & Neck Surgery, Soroka University Medical Center, Beer-Sheva 84105, Israel
4. Dept. of Otorhinolaryngology – Head and Neck Surgery, Turku University and Turku University Hospital

Short title: Role of JNK\c-JUN\AXL pathway in sensitivity to BYL719.

Corresponding authors:

Moshe Elkabets, The Shraga Segal Department of Microbiology, Immunology and Genetics, Ben-Gurion University of the Negev, Beer-Sheva 84105, Israel.
Tel: +972-86428846 FAX: +972-86477626.Email: moshee@bgu.ac.il

Limor Cohen, The Shraga Segal Department of Microbiology, Immunology and Genetics, Ben-Gurion University of the Negev, Beer-Sheva 84105, Israel.
Tel: +972-86428846 FAX: +972-86477626.Email: ayashli@post.bgu.ac.il

Keywords: Esophageal cancer, head and neck cancer, PI3K, AXL, drug resistance, AP-1 complex, c-JUN, JNK inhibition

Conflict of Interest - The authors declare no conflict of interest.

Abstract

AXL overexpression is a common resistance mechanism to anti-cancer therapies, including the p110α isoform specific inhibitor of the phosphoinositide 3-kinase (PI3K), BYL719, in esophagus and head and neck squamous cell carcinoma (ESCC, HNSCC respectively). However, the mechanisms underlying AXL overexpression in resistance to BYL719 remained elusive. Here we demonstrated that the AP-1 transcription factors, c-JUN and c-FOS, regulates AXL overexpression in HNSCC and ESCC. AXL and c-JUN expression is correlated in HNSCC patients, and in HNSCC and ESCC cell lines. Silencing of c-JUN and c-FOS expression in tumor cells reduced AXL expression, and enhanced sensitivity of human papilloma virus positive (HPV^{Pos}) and negative (HPV^{Neg}) tumor cells to BYL719 in vitro. Blocking of the c-JUN N-terminal kinase (JNK), using SP600125, in combination with BYL719 resulted in down-regulation of AXL expression, and potently inhibited mTOR pathway. Synergistic anti-proliferative effect was detected between BYL719 and SP600125 in 15 tumor cell lines in vitro. In-vivo, this drug combination induced tumor growth arrest in cell line and patients-derived xenograft models, and in syngeneic head and neck cancer models. Collectively, our data suggests that JNK inhibition in combination with anti-PI3K therapy is a new therapeutic strategy that may be tested in HPV^{Pos} and HPV^{Neg} HNSCC and ESCC patients.

Introduction

The unsatisfactory outcomes of current therapies for squamous cell carcinoma of head and neck, and esophagus (HNSCC and ESCC, respectively) patients are underscored by the high mortality and morbidity rates of the diseases (1, 2). Taken together with the high incidence rates per year in many countries (3, 4), the development of new therapeutic approaches is urgently needed.

The etiology of HNSCC and ESCC is linked with alcohol consumption and smoking, and in recent years also with the emergence of the human papilloma virus (HPV) infection (Reviewed in (5)). Despite the significant differences in the molecular landscape of HPV-positive (HPV^{Pos}) and HPV-negative (HPV^{Neg}) HNSCC and ESCC (6-8), genomic alterations in the PIK3CA gene are frequent, regardless of HPV status (6-8). PIK3CA encodes for the p110α subunit of the phosphatidylinositol-4,5-bisphosphate 3-kinase (PI3K). Activating point mutations or amplifications of the PIK3CA gene results in the hyper-activation of the PI3K/AKT/mTOR signaling pathway (Review in (9)). This pathway plays a key role in regulating cell proliferation and survival; hence in PIK3CA-mutated HNSCC and ESCC, PI3K enhances tumor progression. Due to the importance of this pathway in HNSCC and ESCC, blockers of the PI3K, AKT and mTOR are under clinical development (Review in (10-12)). Recently, Dejan et al reported that 14 out of 17 PIK3CA- mutated HNSCC patients benefited from a single agent of the isoform specific p110α inhibitor BYL719 (Alpelicib) (13). However, all patients eventually developed resistance to BYL719 (13). We recently showed that the emergence of resistance to BYL719 in HNSCC and ESCC involves the overexpression of the receptor tyrosine kinase (RTK) AXL. AXL dimerizes with epithelial growth factor receptor (EGFR) to signal through the phospholipase Cγ (PLCγ)-protein kinase C (PKC) pathway, leading to the reactivation of mTOR in an AKT independent manner (14). We further showed that AXL overexpression is associated with resistance to BYL719 in patients with HNSCC, and inhibition of AXL using R428 can reverse the resistance to BYL719 (14). AXL seems to be a

central RTK that play a key role in resistance to anti-cancer therapies, as elevated expression of AXL was observed in tumors that became resistance to various therapies (15-19). These evidence emphasize the need to block AXL activity in order to improve drugs efficacies in patients. In fact, blockers of AXL using small molecules or antibodies are under clinical development (ClinicaTtrials.org). However, to the best of our knowledge, targeting the expression of AXL as an alternative therapeutic strategy was not explored yet.

Axl gene transcription was shown to be regulated by several transcription factors (TFs) such as SP1\3 (20) and MZF1 (21) in colon and cervix cancers, and AP-1 complex in melanoma, leukemia and bladder cancers (22-24). However, the TFs that regulate AXL overexpression in ESCC and HNSCC following resistance to PI3K therapy remain uncharacterized. Here we identified the transcriptional machinery that regulates AXL expression in these cancers, and tested new drug combination to limits AXL expression, and to improve the efficacy of BYL719 in vitro and in vivo.

Results

AXL expression determines sensitivity to BYL719 in HPV^{Pos} and HPV^{Neg} cancer cell lines.

We recently showed that AXL overexpression drives acquisition of resistance to BYL719 in cell lines and in HNSCC patients (14). To test if the basal expression of AXL also determines the primary sensitivity to BYL719, we knocked down the expression of AXL in HPV^{Pos} and HPV^{Neg} HNSCC and ESCC cell lines, and measured the half maximal inhibitory concentration (IC:50) of BYL719 in vitro. For HPV^{Neg} cells we used SNU1076 (HNSCC), and our previously established isogenic tumor cell line model, BYL719-sensitive KYSE180 (KYSE180^{Sen}) and their counterpart BYL719-resistant model (KYSE180^{Res}) (ESCC) that showed AXL overexpression (14). For HPV^{Pos} cell line UMSCC47 was used. Knockdown of AXL significantly reduced BYL719 IC:50 values in all tumor cells (Figure 1.A). Western-blot (WB) analysis of the KYSE180^{Sen} tumor cells following treatment with BYL719 showed that AXL expression impact the potency of BYL719 to block mTOR pathway. Specifically, further inhibition of phosphorylation levels of ribosomal protein S6 (pS6), was detected in tumor cells that AXL expression was knocked down (Figure 1.B). These results align with our previous report showing that AXL bypass AKT to active mTOR pathway (14). Next, we confirmed the effect of AXL knockdown on the efficacy of BYL719 in vivo, using a cell line-derived xenograft model (CDX) of KYSE180^{Sen}-shCT and shAXL1 tumor cells. In agreement with the in vitro studies, BYL719 treatment delayed the growth of the shAXL tumors more efficiently compared with shCT tumors (Figure 1.C). This was associated with a reduction in mTOR pathway activation measured by pS6 immunohistochemistry (IHC) staining, and a reduction in tumor cell proliferation, measured by Ki67 IHC (Figure 1.D-E). Similar results were obtained in the HPV^{Pos} UMSCC47–derived CDX model (Supplementary Figure 1.A-D).

Resistance to BYL719 is associated with c-JUN transcription factor upregulation

As the expression level of AXL determined the response of HNSCC and ESCC cells to BYL719, we aimed to identify the molecular machinery that regulates AXL overexpression, using isogenic BYL719-sensitive, and resistant models ($KYSE180^{Sen}$ vs. $KYSE180^{Res}$, $CAL33^{Sen}$ vs. $CAL33^{Res}$) (14). A gene enrichment set analysis of the RNAseq obtained in these cells identified over 100 conserved motifs (padj>0.1X10-5) of 41 TF that were significantly activated (Supplementary Table 1). TCF3, SP-1, AP-1 and MYC were among the most significant TF signatures that were upregulated in both resistant cells. Three of the 41 TF were predicted to have binding sites on AXL promotor (QIAGEN-transcription factor analysis); AP-1, MYC, and MYC Associated Zinc Finger Protein (MAZ) (Figure 2.A). Further analysis of the RNAseq data indicated that the expression levels of MAZ and MYC were similar in BYL719 sensitive vs. resistant cells, whereas the genes of the AP-1 complex; FOSL, FOS and c-JUN were significantly upregulated in both resistant cells models (Supplementary Figure 2.A). WB and qPCR analysis confirmed the upregulation of c-JUN in resistant vs. sensitive cells, which was associated with AXL overexpression (Figure 2.B-C). SP1 transcription factor (previously reported to regulate AXL expression (20, 25)) was upregulated in only in $KYSE180^{Res}$ cells but not in $CAL33^{Res}$ cells. Moreover, we observed an inverse correlation between AXL and microphthalmia-associated transcription factor (MITF) as previously reported for resistance to multiple targeted drugs in melanoma (23, 26, 27) (Figure 2.B). Increased expression of AXL and c-JUN was confirmed in SNU1076 cells that acquired resistant to BYL719 (Supplementary Figure 2. B).

To get further insight on AXL and c-JUN expression at the single cell level, immunofluorescent (IF) staining and imaging flow cytometry were performed. c-JUN and AXL IF-staining showed the upregulation of AXL and c-JUN in BYL719 resistant cells, that were correlated at the single cell level (cells with high AXL displayed high c-JUN levels) (Figure 2.D). Imaging flow cytometry analysis demonstrated that 97% of the $KYSE180^{Sen}$ cells display low expression levels of c-JUN and AXL, and only a small subset of the cells showed high expression

levels of c-JUN that were accompanied by high AXL expression. This trend was reversed in KYSE180^{Res} cells showing co-occurrence of high expression of c-JUN and AXL levels (96.2% of the cells, Supplementary Figure 2.C). Given the positive correlation between AXL and c-JUN, we hypothesized that the AP-1 transcriptional complex, including c-JUN and its counterpart c-FOS regulates AXL expression. Indeed, silencing of c-JUN or c-FOS expression using siRNAs showed a downregulation of AXL protein levels in KYSE180^{Sen}, KYSE180^{Res} SNU1076 cells as measured by WB and qPCR analysis (Figure 2.E and Supplementary Figure 2.D and E). Finally, we performed chromatin immunoprecipitation (ChIP) followed by qPCR to test the binding of c-JUN to the AXL promoter. ChIP of c-JUN showed a slightly increased binding to AXL promoter in KYSE180^{Res} compared to KYSE180^{Sen} (Figure 2.F).

AXL and c-JUN levels are correlated in clinical samples of HNSCC *patients, and in HNSCC and ESCC cell lines.*

To reinforce the role of c-JUN in AXL expression in HNSCC we tested the correlation between AXL and c-JUN in patients with benign (n=15) and malignant (n=17) HNSCC using IHC staining. IHC staining showed a significant increase in both AXL and c-JUN expression in the HNSCC compared to the benign tissues, aligned with previous reports on c-JUN expression in oral SCC (28) (Supplementary Figure 3.C). AXL and c-JUN were positively correlated in HNSCC patients ($R=0.450$, $p=0.0051$, Figure 3.A), and also in the benign tissues ($R=0.6772$, $p<0.0001$, Supplementary Figure 3.B and Supplementary Table 1). Validation of expression of AXL and c-JUN in an independent cohort of 10 freshly isolated HNSCC tumor specimens from Soroka Medical Center were analyzed by WB and by IHC showed a similar trend ($R=0.5254$, $p=0.011$, Figure 3.B). In addition, a positive correlation between AXL and c-JUN expression was detected in 5 HNSCC patient derived xenografts (PDXs) ($R=0.969$, $p=0.0063$, Supplementary Figure 3.D), and in a panel

of 17 HNSCC and ESCC cell lines (R=0.308, p=0.0085, Figure 3.C). The BYL719 IC:50 values of the tested cell lines were also correlated to AXL and c-JUN expression, as most cell lines with high IC:50 values showed high expression levels of AXL and c-JUN (shown by the size of the round symbols in the graph representing each cell line in Figure 3.C, and in Supplementary Figure 3.E). Collectively, the strong positive correlation found between AXL and c-JUN expression in HNSCC and ESCC clinical sample and in cell lines support our finding that AXL expression is transcriptionally regulated by AP-1 complex, which potentially can be a therapeutic target to enhance efficacy of BYL719.

Knockdown of AP-1 members and inhibition of the c-JUN N-terminal kinase enhance BYL719 efficacy in vitro.

As AXL expression is regulated by the AP-1 transcription complex, we hypothesized that c-JUN and c-FOS knockdown will sensitize HNSCC and ESCC cells to BYL719. Indeed, knocking down of c-JUN and c-FOS expression in HPV^{Neg} $KYSE180^{Sen}$, $KYSE180^{Res}$ and SNU1076 cells using RNAi significantly reduced the IC:50 values of BYL719. These results were also validated in HPV^{Pos} cell lines USCC60A and UMSCC47 (Figure 4.A and Supplementary Figure 4.A).

The direct role of c-JUN/c-FOS in AXL expression and in BYL719 sensitivity in HNSCC and ESCC cell lines suggests that blocking of c-JUN activity may potentiate BYL719 efficacy. As direct blockers of c-JUN are not yet available, we tested the inhibitor of c-JUN N-terminal kinase (JNK), SP600125 (29). The combination of BYL719 and SP600125 significantly decreased the IC:50 values of BYL719 in five HPV^{Pos} and HPV^{Neg} HNSCC and ESCC cell lines (Figure 4.B and Supplementary Figure 4.B). Notably, $KYSE180^{Res}$ cells were sensitized to BYL719 using SP600125 to similar IC:50 values as $KYSE180^{Sen}$ cells, suggesting that the combined treatment may inhibit the emergence of resistance. A cell proliferation assay monitoring growth rates of the cells showed that

the combined treatment of BYL719 and SP600125 had a superior anti-proliferative effect, and potentially cell death in HPV^{Pos} SCC60A cell line (Supplementary Figure 4.C). WB analysis showed that while BYL719 upregulated AXL expression, its combination with SP600125 (10μM) decreased AXL protein levels (Figure 4.C). The level pS6, was further inhibited by the combination of BYL719 and SP600125 in $KYSE180^{Res}$ and SNU1076 cells. A qPCR analysis showed that AXL mRNA levels were initially increased following BYL719 treatments in $KYSE180^{Sen}$, SNU1076 and SCC60A cells, and the combination with SP600125 decreased AXL mRNA levels compared with BYL719 alone (Figure 4.D). In $KYSE180^{Res}$ cells, where AXL transcript basal levels of were stably elevated (Figure 2.C), a significant down regulation of AXL mRNA levels following SP600125 was also detected.

To explore if BYL719 and SP600125 have an additive or synergistic anti-proliferative effect, a synergy test was performed in five- $PIK3CA^{mut}$, three- $PIK3CA^{wt}$ (all HPV^{Neg}) HNSCC and ESCC cell line, and five- HPV^{pos} HNSCC cell lines. Representative images of the analysis in SNU1076 cells are presented in Supplementary Figure 4.D. Calculation of the synergy score using the Chalice^{TM} software indicated a synergistic effect (>1) in 15 of 17 cell lines tested, whereas an additive effect was observed in the BYL719 acquired-resistant cell lines $KYSE180^{Res}$ and $CAL33^{Res}$ cell lines(figure 4.E).

Superior efficacy of a combined treatment with BYL719 and SP600125 in vivo

To explore the efficacy of BYL719 and SP600125 combination in vivo, CDX models of $KYSE180^{Sen}$ (HPV^{Neg}) and UTSCC47 (HPV^{Pos}) cells were created, and tumor growth was measured. Daily treatments of mice with monotherapy of BYL719 (25 mg/kg) delayed tumor growth compared to vehicle treatment. However, a significant tumor growth arrest (in HPV^{Neg} $KYSE180^{Sen}$ CDXs) and tumor shrinkage (in HPV^{Pos} UTSCC47 CDXs) were observed in mice treated with the combination of BYL719 and SP600125 (Figure 5. A-B, Supplementary Figure 5.A-B). We did not

detect any toxicity, as mice weight remained stable (Supplementary Figure 5.A-B). IHC staining of the proliferation marker, Ki67, showed a decreased tumor cell proliferation in tumors treated with BYL719 and SP600125 monotherapy. However, a greater inhibition of cells proliferation was detected in tumors treatment with the combination.

To further validate our observation in pre-clinical models, the efficacy of drug combination was tested in two PDX models (SE1 and SE3). Treatments of mice with the combination of BYL719 and SP600125 showed a superior anti-tumor effect as shown by tumor volumes and tumor weights (Figure 5.C and Supplementary Figure 5.C). Changes in tumor volumes indicated a stable disease in mice treated with BYL719 and SP600125 combination, while only tumor growth delay was observed in mice treated with monotherapies. Ki67 staining showed a similar trend, further supporting the potency of drug combination.

Enhanced anti-tumor efficacy of BYL719 and SP600125 prevents tumor progression and enhances survival in syngeneic head and neck cancers

To further verify our findings in syngeneic HNSCC tumors, we developed HPV^{Neg} tumors, and explored the efficacy of BLY719 and SP600125 in C57BL/6 mice. Lips and tongue squamous cell carcinoma tumors developed following exposure of C57BL6/c mice to the carcinogen 4NQO in the drinking water as previously reported (30) (Supplementary Figure 6.A). IHC analysis of the 4NQO-induced-tongue cancer showed that in malignant lesion (Ki67 and KRT14 positive staining), the AKT pathway is active, and that AXL and c-JUN are expressed in cancer cells (Figure 6.A). Following generation of two cell lines derived from the lips and tongue tumors, we studied the efficacy of BYL719 and SP600125 in vitro and in vivo. In vitro, tumor cell proliferation studies showed that BYL719 and SP600125 combination had a superior anti-proliferative activity, which was associated with a reduction of pS6 levels as shown by WB analysis (Figure 6.B-C). In vivo, the

efficacy of the drugs combination had a significant anti-tumor effect in two syngeneic cancer models. Lips tumors displayed a stable disease in mice treated with BYL719 and SP600125 combination, compared with tumor progression mice treated with either BYL719 or SP600125 (Figure 6.E). In an orthotropic tongue cancer model, BYL719 and SP600125 combination significantly improved the survival of the mice. The median survival for vehicle and SP600125 treated mice was 16 and 17 days, respectively, and for BYL719 treated mice, 23.5 days. However, the median survival of mice in the combination group was 52 days. MRI imaging supported the finding, as drugs combination delayed tumor progression (Figure 6.D).

Discussion

In this work, we demonstrated that AXL levels determine the sensitivity of HPV^{Neg} and HPV^{Pos} HNSCC and ESCC cells to BYL719. We identified the AP-1 transcriptional complex as a regulator of AXL expression in these diseases, and demonstrated that JNK inhibition enhances the anti-tumor efficacy of BYL719 in vitro and in vivo (Scheme 1).

The rationale for targeting the PI3K pathway in several malignancies including in head and neck cancer, using isoform specific inhibitors was well demonstrated (13, 31-37). The first clinical trial testing the p110α isoform specific inhibitor BYL719, showed encouraging results in $PIK3CA_{mut}$ head and neck cancer (13). The major obstacle in implementing BYL719 in HNSCC and ESCC is the primary and the acquired-resistance that is driven by the overexpression of AXL (14). This overexpression of AXL in response to therapy is not exceptional to either these malignant diseases or to PI3K therapies, as other cancer types developed resistance to radiotherapy, chemotherapies and EGFR inhibitors via AXL pathway activation (15-19, 38-40). Hence, targeting AXL receptor and its pathway using the small molecule inhibitors (such as BGB324, ONO-747, TP-0903, MGCD516 and BPI-9016M) or specific antibodies (CAB-AXL-ADC) are under clinical evaluation in 14 clinical trials as monotherapy or in combination with other therapies in different settings (clinicaltrials.gov). The clinical outcomes of these studies are not yet available, but pre-clinical models indicate that the efficacy of a single agent of AXL therapies can be limited by expression of other receptors like MERTK (41), while in combination, the potency is enlarged (15, 40, 42-47).

Here we took an alternative approach to reduce availability of AXL by limiting its transcription. Initially, we demonstrated that AXL levels determine the efficacy of BYL719 in HNSCC and ESCC cells in vitro and in vivo, which supported the rationale to reduce AXL expression in tumor cells in order to enhance BYL719 efficacy. This observation is applicative to HPV^{Pos} and HPV^{Neg} HNSCC and ESCC, which may overcome the primary resistance to BYL719 reported recently in HPV^{Pos} cells

(48). We gained an additional confidence for our approach to reduce AXL expression level as a therapeutic opportunity, as Wheeler's group showed that reduction of AXL expression enhances the efficacy of cetuximab in HPV^{Pos} and HPV^{Neg} HNSCC tumors (15, 49).

AXL overexpression in response to therapeutic stress can evolve through several mechanisms such as transcriptional regulation (50, 51) (52) (15, 23, 24), post-translational regulation (53, 54), and expression of miRNA (55) (Reviewed in (56)). In our isogenic tumor cell line of BYL719-sensitive and acquired-resistant cells, we observed a concomitant increase of AXL and AP-1 members expression in resistant cells. Thus, we hypothesized that overexpression of AXL is regulated by the AP-1 transcription factor complex. Indeed, knockdown of AP-1 members (FOS and c-JUN) in tumor cells resulted in a significant reduction in AXL protein and mRNA expression levels.

The mechanism by which BYL719 induces the activation of AP-1 complex is not yet clear, however, the reverse expression of MITF and c-JUN in the $KYSE180^{Res}$ and $CAL33^{Res}$ cells may shed light on a potential role of cytokines in this process. Because MITF is known to prevent c-JUN expression via binding to the c-JUN regulatory genomic region, down regulation of MITF expression following pro inflammatory cytokines secretions, resulted in c-JUN overexpression (57). As it was shown that PI3K inhibition upregulated the secretion of pro-inflammatory cytokines secretion like TNFα (57-59), it is tempting to suggest that BYL719 treatment induces pro-inflammatory cytokines secretion that will down regulate MITF expression, and by that activate c-JUN and AXL expression. Recent paper by Guo et al, reinforced the link of TNFα\c-JUN\AXL axis in resistance to EGFRi in glioblastoma cells(45).

In an attempt to target c-JUN induced-AXL expression, and as direct c-JUN inhibitors are not available, we tested an inhibitor of JNK activation- SP600125 (29). Supplementation of SP600125 to BYL719 improved BYL719 anti-proliferative affect in vitro, to a similar degree as silencing of c-JUN using RNAi. The combined treatment of BYL719 and SP600125 showed an additive or

synergistic anti-proliferative effect in 15 cell lines tested. Due to the nature of drugs synergy effect we used relatively low dosage of BYL719 and SP600125 (25mg\kg and 15mg\kg daily, respectively) in mice. These low drug concentrations prevented tumor progression with no evidence of toxicity.

Targeting the AP-1 or c-JUN signaling may have a broader effect on tumor cells beyond AXL expression. Blocking the pleotropic role of AP-1 TF expression in HNSCC may affect cancer stem cells (60), epithelial-mesenchymal transition (61), and tumor invasiveness (62). Additionally, blocking AP-1 transcription activity may influence the expression of key RTKs like EGFR (63, 64). Lastly, blocking AP-1 complex can also reduce the expression of the immuno-suppressor modulator of PD-L1 (65), and enhance tumor elimination. This possibility is also supported by the notion that AXL and PD-L1 expression are correlated in different cancers (66, 67), and in TCGA data set of head and neck cancer (data not shown). However, further analysis need to be conducted to confirm this hypothesis in our model.

In summary, we present solid evidence that upregulation of AXL in PI3K-resistance cells is regulated by the AP-1 transcription factors. Knockdown of AXL or AP-1 resulted in enhance anti-tumor efficacy of BYL719. Targeting of JNK using SP600125 together with BYL719 had a potent anti-tumor activity against HPV^{Pos} and HPV^{Neg} cells. Such results provide a strong rationale to investigate these drug combinations in HNSCC and ESCC patients.

Material and Methods

Tumor Cell Lines

All HPV^{Neg} cell lines were purchased from commercial vendors. Cell lines sources and specific media is presented in Supplementary materials and methods.

$KYSE180^{Res}$ and $CAL33^{Res}$ cell lines that were BYL719 resistant were developed previously (14), and SNU1076 resistant cell lines was developed using the same approach as previously described (14).

All HPV^{Pos} cell lines were kindly provided by Prof. Reidar Grénman, Turku University, Finland, and grown in DMEM medium.

Two mice HNSCC cell lines were developed in our lab, from 4NQO-induced oral cancer. Briefly, fresh lips and tongue tumor tissues were washed with Hank's balanced salt solution (HBSS) or PBS, cut into small pieces with sterile scissors, and treated with an enzyme mix of Collagenase [10 mg/ml] Hyaluronidase [1 mg/ml] DNase [200 U/ml]. The tissues were dissociated using the *gentleMACS™ Dissociator*. Cells were filtered through a 70µM cell strainer, centrifuged (1500rpm, 5 min) and cultured.

All cells were maintained at 37°C, in a humidified atmosphere at 5% CO_2, in the relevant medium supplemented with 1% L-glutamine 200mM, 100 units of penicillin and streptomycin 10% fetal bovine serum. For Acquired resistance cell lines, 2µM of BYL719 was added to the medium every 5 days.

Cells were routinely tested for mycoplasma infection, and treated with appropriate antibiotics as needed. (De-Plasma™ , TOKU-E, D022). HPV^{Neg} cells were tested for cell line authentication in our previous work (14) and several cell lines (SNU1076, FADU, HSC-2 and HSC-4) were re-tested in this work.

Western Blotting

Cells were washed with ice-cold Phosphate buffered saline (PBS), harvested into lysis buffer (50 mM HEPES, pH 7.5, 150 mM NaCl, 1 mM EDTA, 1 mM EGTA, 10% glycerol, 1% Triton X-100, 10 µM MgCl2), supplemented with phosphatase inhibitor cocktails (Biotool Cat. B15001A/B) and

protease inhibitor (Sigma-Aldrich Cat. P2714-1BTL) and placed on ice for 30 minutes, followed by 3 minutes of ultrasonic cell disruption. Lysates were cleared by centrifuge (30 min,14,000 rpm, 4°C). Supernatants were collected, protein concentrations were determined using Bio-Rad protein assay, SDS sample buffer was added, and samples were boiled for 5 min and then frozen at −80°C until used. Whole cell lysates (25 µg) were separated on 10% SDS–PAGE and blotted onto PVDF membranes (BioRad trans blot® Turbo™ transfer pack #1704157). Membranes were blocked for 1 hour in blocking solution (5% BSA (Amresco 0332-TAM) in Tris-buffered saline (TBS) with 0.1% tween) and then incubated with primary antibodies diluted in blocking solution. Mouse and rabbit horseradish peroxidase (HRP)-conjugated secondary antibodies were diluted in blocking solution. Protein-antibody complexes were detected by chemiluminescence (Westar Supernova, Cyanagen Cat. XLS3.0100) and Westar Nova 2.0 (Cyanagen Cat. XLS071.0250), and images were captured using the Azure C300 Chemiluminescent Western Blot Imaging System, Azure Biosystems. Antibodies detail, and dilutions used:

Real-time PCR

Total RNA was isolated from the cultured cells using PureLink™ RNA Mini Kit (Invitrogen, Thermo Fisher Scientific) according to the manufacturer's protocol. 1 µg RNA was converted to cDNA using qScript™ cDNA synthesis kit (Quanta bioscience, 95047-100) according to the manufacturer's protocol. Real-time PCR was preformed (Roche light cycler 480 II) using PrimeTime Gene Expression Master Mix (IDT Cat. 1055770), with matching probes from IDT: For Axl gene Hs.PT.56a.1942285, GAPH Hs.PT.39a.22214836, Jun Hs.PT.58.25094714.g, Fos Hs.PT.58.15540029. Analysis was done in the light cycler 480 sw 1.5.1 software. Fold change was calculated using the ΔΔCt method. Results were normalized to GAPDH levels and presented as a fold increase of the control cells.

Gene enrichment set analysis

715 genes were upregulated in resistant cells compared to sensitive cells (cut off of >100 reads, and > of 0.5Log2, padj >0.05). Gene enrichment set analysis was performed using GESA of the broad institute (http://software.broadinstitute.org/gsea/index.jsp). For conserved motif the threshold defined as (padj>0.1X10-5). For binding site of AXL promoter we used the the Genecard and the Transcription factor binding sites by QIAGEN websites. All the data is available in supplementary table 1

Immunohistochemistry (IHC) and Immunofluorescence (IF).

Tissues were fixed in a 4% PFA solution for a maximum of 24 hours at room temperature, dehydrated and embedded in paraffin. The tissue sections were de-paraffinzed with xylene. 3%. H_2O_2 was used to block the endogenous peroxidase activity for 20 minutes and rinsed in water for 5 minutes. Antigen retrieval was performed in citrate buffer (pH 6) at 99.99°C, 5 minutes. Sections were then blocked for 1 hour at room temperature with blocking solution (PBS, 0.1%TWEEN (0.0125% for AXL staining), 5% BSA), followed by incubating with primary antibody (diluted in blocking solution) overnight in 4°C. The ABC kit (VECTASTAIN Cat. VE-PK-6200) was used for detection according to manufacturer protocol. Sections were counter stained with hematoxylin and mounted with mounting media (Micromount ,Leica Cat. 380-1730).

For IF, cells were seeded on 8 well glass slides (Cellvis, Cat no. C8-1.5H-N) for 48h. Cells were rinsed with cold PBS (4°C) and fixated in 4% paraformaldehyde for 30 minutes at room temperature. Cells were then rinsed with PBS followed by permeabilization on ice for 5 minutes in PBS with 0.05% Triton X-100 (Sigma-Aldrich), rinsed with PBS, and blocked in blocking solution for 30 min at room temperature (5% BSA in Tween-PBS). The cells were incubated with primary antibodies overnight in 4°C, rinsed with PBS, and incubated with Cy3 conjugated anti-rabbit secondary antibody (1:250) (Jackson ImmunoResearch, 111-165-144) and Alexa FluorÂ 488-conjugated anti-mouse secondary antibody (1:250) (Jackson ImmunoResearch, 115-545-062), at room temperature for 1 hour. Cells were then rinsed with PBS and mounted using Dapi Fluoromount-G® (SouthenBiotech, 0100-20).

IHC and IF slides were digitalized using the Pannoramic Scanner (3DHISTECH, Budapest, Hungary) and analyzed using QuantCenter (3DHISTECH, Budapest, Hungary) using a single threshold parameter for all images of a specific staining in each experiment.

Tissue Microarray

Tissue microarray slides containing 17 HNSCC and 15 benign tumors were purchased from US Biomax (HNT961). The information of these samples and the level of AXL and c-JUN was summarized in Supplementary Table 2.

IC:50 and synergy assay

Cells were seeded in 96-well plates (3000 cells per well), treated with increasing concentration of indicated drugs (0-10μM), and allowed to proliferate for 4 days. Cells were then fixed using Trichloroacetic acid (TCA) 0.6M for 1 hour at 4°C and rinsed, and stained with Crystal Violet (1g/L) for 30 minutes, in room temperature. Crystal violet was dissolved using 10% acetic acid and absorbance was measured at 570nm in a spectrophotometer (Epoch, biotech). IC:50 values were calculated using the GraphPad Software. For synergy assay, the proliferation of the cells in the different treatment groups was presented as a percentage of control (DMSO treated) cells, and the percent of growth inhibition was calculated. Synergy scores were analyzed using Chalice™ Bioinformatics Software (http://cwr.horizondiscovery.com) (68) and the synergistic effects were calculated based on the statistic Loewe Excess model and the equation: S = fcov ln fX ln fY ∑ max(0,Idata) max(0,Idata–ILoewe).

siRNA and shRNA

For transient silencing of c-JUN and c-FOS, cells were transfected using GenMute® siRNA Transfection Reagent (SignaGen Cat. SL100568) according to manufacturer's protocol, with a siRNA non-targeting control sequence (IDT, Cat. 51-01-14-04), and a c-JUN or c-FOS gene targeting sequence (IDT, Cat. hs.Ri.JUN.13 and hs.Ri.FOS.13.1, respectively). Cells were harvested following 48hr for WB and qPCR analysis, or treated with the indicated drugs for IC:50 experiments following 24hr.

For the creation of shRNAs cell lines, we created lentiviruses by transfecting HEK293 cells with the viral plasmids psPAX2, pMD2.G, and PLKO with shRNAs – a control scrambled sequence (shCT), or 2 different sequences for the silencing of AXL expression (shAXL1 and shAXL2, MSKCC RNAi core facility identifiers TRCN0000001037 and TRCN0000194771, respectively) using PolyJet transfection reagent (SignaGen, Cat. SL100688). Viruses were collected following 48-72hr and used for cell infection. Cells were seeded in a 6 well plate (150000 cells per well) and infected with the lentiviruses in the presence of polybrene (Sigma Aldrich Cat. 5G-H9268). Cells were selected using puromycin (Gibco Cat. A11138-03).

Cell proliferation assay

Cells were seeded in a 24 well plate (10,000 cells per well), and treated as indicated. The real time cell history recorder JULI^{TM} Stage was used to record cell confluence every 6 hrs. Results are presented as the averaged confluence ±SEM. For the 4NQO-induced cell lines (Figure 6.B), cells were treated as indicated for 4 days and then fixed and stained with crystal violet. Results are presented as a percentage of the control (DMSO) treated cells.

Chromatin immunoprecipitation assay (ChIP)

ChIP experiments were performed using the Magna ChIP^{TM} A (Merck, Catalog # 17-610), according to the manufacturer protocol. KYSE180^{Sen} and KYS180^{Res} cells were cultured in 145mm plates and grown for 48h. Chromatin-proteins were crosslinked, extracted, and fragmented to 150-300b.p using sonication. DNA was then immunopercipitated with c-JUN antibody (1:50, CST, Cat. 9165S), or IgG control (1:50 CST, Cat. 3900) over night at 4^0C. QPCR was performed for the enrichments of AXL promotor in c-JUN IP samples, using SYBR Green FastMix (QuantaBio Cat. 95072-250-2), and primers for the AP-1 binding site on the AXL promoter :5'- AGT GTG TCT GTG GGC CAG TA-3' and 5'-CCT TCA TTC CCC CTC ACT CT-3' (20977427).

Establishment of Tumor Xenografts and Studies in Mice

NOD.CB17-Prkdc-scid/NCr Hsd mice were purchased from Envigo. Mice were maintained and treated according to the institutional guidelines of Ben-Gurion University of the Negev. Mice were housed in air-filtered laminar flow cabinets with a 12 hours light/dark cycle and food and water ad libitum. Animal experiments were approved by the institutional animal care and use committees (IL.80-12-2015).

For cell-line-derived xenografts (CDXs), 6-week-old mice were injected subcutaneously in the flunk with $2x10^6$ cells in 200µl PBS (100µl in each side). Tumors developed following around 2 weeks ($60mm^3$).

Patient-derived xenografts (PDXs) were established from HNSCC patients, from the Ear, Nose, and Throat unit, Soroka Medical Center, Israel. All patients signed an informed consent. All PDXs were first transplanted into the flunk of 6-week-old NOD.Cg-Prkdc Il2rg/SzJ (Jackson labs) subcutaneously within 24 hours after surgery, and after establishment and expansion, re-transplanted

to NOD.CB17-Prkdc-scid/NCr Hsd mice for drug efficacy experiments, and following around 2 weeks randomized to four groups, with n = 6–8 mice per group.

For carcinogen induced HNSCC in C57BL/6 immunocompetent mice (Envigo), mice were given 50 µg/mL 4-nitroquinoline 1-oxide (4-NQO) in their drinking water for 3-4 months, and tumors developed following 2 month (Supplementary figure 6.A). We developed a syngeneic lips tumor model by transplanting lips tumors in the flunk of syngeneic mice. For survival experiments an orthotopic model was developed by injecting $0.5x10^6$ 4NQO- tongue cell line in the tongue of syngeneic mice. Animals were randomized to 4 groups with n=10-12 tumors per group, at a tumor volume of 70 to 120 mm^3**,** 2-4 weeks after implantation.

Animals were orally treated with vehicle (corn oil, 4% DMSO that was used for SP600125 administration and 0.5% carboxymethyl cellulose that was used for BYL719 administration), BYL719 (25 mg/kg) and/or JNK inhibitor SP600125 (15 mg/kg) daily. Tumors were measured with digital caliper twice a week, and tumor volumes were determined with the formula: $Length \times width^2 \times \frac{\pi}{6}$. At the end of the experiment**,** animals were sacrificed using CO2 inhalation and the tumors were harvested for investigation. Tumor volumes were normalized to initial volumes and presented as an averaged percentage of the initial volumes ± SEM

Drugs

BYL719 was kindly provided by Novartis and dissolved in DMSO (Sigma Aldrich cat. D8418) for in vitro experiments or 0.5% carboxymethyl cellulose (Sigma Aldrich cat. 9481-1KG) for in vivo administration. SP600125 was purchased from Fluorochem (Cat. M02529) and dissolved in for in vitro assays, or corn oil (Sigma Aldrich cat. C8267-500ML) with 4% DMSO.

Statistical Analysis

Experiments were repeated at least three times and representative data/images are shown. Statistical analysis was performed using GraphPad Prism software, presented as mean ± SEM. For comparisons between two groups, P values were calculated. P values of 0.05 (*), 0.01 (**), 0.001 (***) were considered statistically significant

Author contributions

M.B, M.P, L.C and M.E designed research studies, M.B, M.P, L.C conducted experiments, acquired data and analyzed. J.B, A.B.D and R.G. providing clinical samples and cell lines. M.E, L.C and M.B, wrote the manuscript.

Acknowledgments

This work was funded by the Israel Science Foundation (ISF, 700/16) to M.E., the INCPM (1901/17) to ME, Concern Foundation (#876571) to M.E. . M.E is supported by the Alon Fellowship for outstanding young researcher. M.B is supported by the VATA- for excellent students.

References

1. Wiegand S, Zimmermann A, Wilhelm T, and Werner JA. Survival After Distant Metastasis in Head and Neck Cancer. *Anticancer Res.* 2015;35(10):5499-502.
2. Ferlay J, Soerjomataram I, Dikshit R, Eser S, Mathers C, Rebelo M, Parkin DM, Forman D, and Bray F. Cancer incidence and mortality worldwide: sources, methods and major patterns in GLOBOCAN 2012. *Int J Cancer.* 2015;136(5):E359-86.
3. Curado MP, and Hashibe M. Recent changes in the epidemiology of head and neck cancer. *Curr Opin Oncol.* 2009;21(3):194-200.
4. Marur S, D'Souza G, Westra WH, and Forastiere AA. HPV-associated head and neck cancer: a virus-related cancer epidemic. *The Lancet Oncology.* 2010;11(8):781-9.
5. Argiris A, Karamouzis MV, Raben D, and Ferris RL. Head and neck cancer. *Lancet.* 2008;371(9625):1695-709.
6. Cancer Genome Atlas N. Comprehensive genomic characterization of head and neck squamous cell carcinomas. *Nature.* 2015;517(7536):576-82.
7. Seiwert TY, Zuo Z, Keck MK, Khattri A, Pedamallu CS, Stricker T, Brown C, Pugh TJ, Stojanov P, Cho J, et al. Integrative and comparative genomic analysis of HPV-positive and HPV-negative head and neck squamous cell carcinomas. *Clinical cancer research : an official journal of the American Association for Cancer Research.* 2015;21(3):632-41.
8. Stransky N, Egloff AM, Tward AD, Kostic AD, Cibulskis K, Sivachenko A, Kryukov GV, Lawrence MS, Sougnez C, McKenna A, et al. The mutational landscape of head and neck squamous cell carcinoma. *Science.* 2011;333(6046):1157-60.
9. Cantley LC. The phosphoinositide 3-kinase pathway. *Science.* 2002;296(5573):1655-7.
10. Courtney KD, Corcoran RB, and Engelman JA. The PI3K pathway as drug target in human cancer. *Journal of clinical oncology : official journal of the American Society of Clinical Oncology.* 2010;28(6):1075-83.
11. Engelman JA. Targeting PI3K signalling in cancer: opportunities, challenges and limitations. *Nature reviews Cancer.* 2009;9(8):550-62.
12. Rodon J, Dienstmann R, Serra V, and Tabernero J. Development of PI3K inhibitors: lessons learned from early clinical trials. *Nat Rev Clin Oncol.* 2013;10(3):143-53.
13. Juric D, Rodon J, Tabernero J, Janku F, Burris HA, Schellens JHM, Middleton MR, Berlin J, Schuler M, Gil-Martin M, et al. Phosphatidylinositol 3-Kinase alpha-Selective Inhibition With Alpelisib (BYL719) in PIK3CA-Altered Solid Tumors: Results From the First-in-Human Study. *Journal of clinical oncology : official journal of the American Society of Clinical Oncology.* 2018;36(13):1291-9.
14. Elkabets M, Pazarentzos E, Juric D, Sheng Q, Pelossof RA, Brook S, Benzaken AO, Rodon J, Morse N, Yan JJ, et al. AXL mediates resistance to PI3Kalpha inhibition by activating the EGFR/PKC/mTOR axis in head and neck and esophageal squamous cell carcinomas. *Cancer cell.* 2015;27(4):533-46.
15. Brand TM, Iida M, Stein AP, Corrigan KL, Braverman CM, Luthar N, Toulany M, Gill PS, Salgia R, Kimple RJ, et al. AXL mediates resistance to cetuximab therapy. *Cancer research.* 2014;74(18):5152-64.
16. Dufies M, Jacquel A, Belhacene N, Robert G, Cluzeau T, Luciano F, Cassuto JP, Raynaud S, and Auberger P. Mechanisms of AXL overexpression and function in Imatinib-resistant chronic myeloid leukemia cells. *Oncotarget.* 2011;2(11):874-85.
17. Giles KM, Kalinowski FC, Candy PA, Epis MR, Zhang PM, Redfern AD, Stuart LM, Goodall GJ, and Leedman PJ. Axl mediates acquired resistance of head and neck cancer cells to the epidermal growth factor receptor inhibitor erlotinib. *Molecular cancer therapeutics.* 2013;12(11):2541-58.
18. Hong J, and Belkhiri A. AXL mediates TRAIL resistance in esophageal adenocarcinoma. *Neoplasia.* 2013;15(3):296-304.
19. Zhang Z, Lee JC, Lin L, Olivas V, Au V, LaFramboise T, Abdel-Rahman M, Wang X, Levine AD, Rho JK, et al. Activation of the AXL kinase causes resistance to EGFR-targeted therapy in lung cancer. *Nature genetics.* 2012;44(8):852-60.

20. Mudduluru G, and Allgayer H. The human receptor tyrosine kinase Axl gene--promoter characterization and regulation of constitutive expression by Sp1, Sp3 and CpG methylation. *Bioscience reports.* 2008;28(3):161-76.
21. Mudduluru G, Vajkoczy P, and Allgayer H. Myeloid zinc finger 1 induces migration, invasion, and in vivo metastasis through Axl gene expression in solid cancer. *Mol Cancer Res.* 2010;8(2):159-69.
22. Mudduluru G, Leupold JH, Stroebel P, and Allgayer H. PMA up-regulates the transcription of Axl by AP-1 transcription factor binding to TRE sequences via the MAPK cascade in leukaemia cells. *Biology of the cell / under the auspices of the European Cell Biology Organization.* 2010;103(1):21-33.
23. Maurus K, Hufnagel A, Geiger F, Graf S, Berking C, Heinemann A, Paschen A, Kneitz S, Stigloher C, Geissinger E, et al. The AP-1 transcription factor FOSL1 causes melanocyte reprogramming and transformation. *Oncogene.* 2017;36(36):5110-21.
24. Sayan AE, Stanford R, Vickery R, Grigorenko E, Diesch J, Kulbicki K, Edwards R, Pal R, Greaves P, Jariel-Encontre I, et al. Fra-1 controls motility of bladder cancer cells via transcriptional upregulation of the receptor tyrosine kinase AXL. *Oncogene.* 2012;31(12):1493-503.
25. Zhen Y, Lee IJ, Finkelman FD, and Shao WH. Targeted inhibition of Axl receptor tyrosine kinase ameliorates anti-GBM-induced lupus-like nephritis. *J Autoimmun.* 2018.
26. Konieczkowski DJ, Johannessen CM, Abudayyeh O, Kim JW, Cooper ZA, Piris A, Frederick DT, Barzily-Rokni M, Straussman R, Haq R, et al. A melanoma cell state distinction influences sensitivity to MAPK pathway inhibitors. *Cancer discovery.* 2014;4(7):816-27.
27. Muller J, Krijgsman O, Tsoi J, Robert L, Hugo W, Song C, Kong X, Possik PA, Cornelissen-Steijger PD, Geukes Foppen MH, et al. Low MITF/AXL ratio predicts early resistance to multiple targeted drugs in melanoma. *Nat Commun.* 2014;5(5712.
28. Xu H, Jin X, Yuan Y, Deng P, Jiang L, Zeng X, Li XS, Wang ZY, and Chen QM. Prognostic value from integrative analysis of transcription factors c-Jun and Fra-1 in oral squamous cell carcinoma: a multicenter cohort study. *Sci Rep.* 2017;7(1):7522.
29. Bennett BL, Sasaki DT, Murray BW, O'Leary EC, Sakata ST, Xu W, Leisten JC, Motiwala A, Pierce S, Satoh Y, et al. SP600125, an anthrapyrazolone inhibitor of Jun N-terminal kinase. *Proceedings of the National Academy of Sciences of the United States of America.* 2001;98(24):13681-6.
30. Hawkins BL, Heniford BW, Ackermann DM, Leonberger M, Martinez SA, and Hendler FJ. 4NQO carcinogenesis: a mouse model of oral cavity squamous cell carcinoma. *Head & neck.* 1994;16(5):424-32.
31. Rodon J, Juric D, Gonzalez-Angulo A-M, Bendell J, Berlin J, Bootle D, Gravelin K, Huang A, Derti A, Wuerthner JLJ, et al. *Annual meeting AACR 2013*. 2013.
32. Elkabets M, Vora S, Juric D, Morse N, Mino-Kenudson M, Muranen T, Tao J, Campos AB, Rodon J, Ibrahim YH, et al. mTORC1 Inhibition Is Required for Sensitivity to PI3K p110alpha Inhibitors in PIK3CA-Mutant Breast Cancer. *Science translational medicine.* 2013;5(196):196ra99.
33. Fritsch C, Huang A, Chatenay-Rivauday C, Schnell C, Reddy A, Liu M, Kauffmann A, Guthy D, Erdmann D, De Pover A, et al. Characterization of the novel and specific PI3Kalpha inhibitor NVP-BYL719 and development of the patient stratification strategy for clinical trials. *Molecular cancer therapeutics.* 2014;13(5):1117-29.
34. Furet P, Guagnano V, Fairhurst RA, Imbach-Weese P, Bruce I, Knapp M, Fritsch C, Blasco F, Blanz J, Aichholz R, et al. Discovery of NVP-BYL719 a potent and selective phosphatidylinositol-3 kinase alpha inhibitor selected for clinical evaluation. *Bioorganic & medicinal chemistry letters.* 2013;23(13):3741-8.
35. Zumsteg ZS, Morse N, Krigsfeld G, Gupta G, Higginson DS, Lee NY, Morris L, Ganly I, Shiao SL, Powell SN, et al. Taselisib (GDC-0032), a Potent beta-Sparing Small Molecule Inhibitor of PI3K, Radiosensitizes Head and Neck Squamous Carcinomas Containing Activating PIK3CA Alterations. *Clinical cancer research : an official journal of the American Association for Cancer Research.* 2016;22(8):2009-19.
36. De Felice F, and Guerrero Urbano T. New drug development in head and neck squamous cell carcinoma: The PI3-K inhibitors. *Oral oncology.* 2017;67(119-23.

37. Mizrachi A, Shamay Y, Shah J, Brook S, Soong J, Rajasekhar VK, Humm JL, Healey JH, Powell SN, Baselga J, et al. Tumour-specific PI3K inhibition via nanoparticle-targeted delivery in head and neck squamous cell carcinoma. *Nat Commun.* 2017;8(14292.
38. Liu L, Greger J, Shi H, Liu Y, Greshock J, Annan R, Halsey W, Sathe GM, Martin AM, and Gilmer TM. Novel mechanism of lapatinib resistance in HER2-positive breast tumor cells: activation of AXL. *Cancer research.* 2009;69(17):6871-8.
39. Byers LA, Diao L, Wang J, Saintigny P, Girard L, Peyton M, Shen L, Fan Y, Giri U, Tumula PK, et al. An epithelial-mesenchymal transition gene signature predicts resistance to EGFR and PI3K inhibitors and identifies Axl as a therapeutic target for overcoming EGFR inhibitor resistance. *Clinical cancer research : an official journal of the American Association for Cancer Research.* 2013;19(1):279-90.
40. Brand TM, Iida M, Stein AP, Corrigan KL, Braverman CM, Coan JP, Pearson HE, Bahrar H, Fowler TL, Bednarz BP, et al. AXL Is a Logical Molecular Target in Head and Neck Squamous Cell Carcinoma. *Clinical cancer research : an official journal of the American Association for Cancer Research.* 2015;21(11):2601-12.
41. McDaniel NK, Cummings CT, Iida M, Hulse J, Pearson HE, Vasileiadi E, Parker RE, Orbuch RA, Ondracek OJ, Welke NB, et al. MERTK mediates intrinsic and adaptive resistance to AXL-targeting agents. *Molecular cancer therapeutics.* 2018.
42. Balaji K, Vijayaraghavan S, Diao L, Tong P, Fan Y, Carey JP, Bui TN, Warner S, Heymach JV, Hunt KK, et al. AXL Inhibition Suppresses the DNA Damage Response and Sensitizes Cells to PARP Inhibition in Multiple Cancers. *Mol Cancer Res.* 2017;15(1):45-58.
43. Ben-Batalla I, Erdmann R, Jorgensen H, Mitchell R, Ernst T, von Amsberg G, Schafhausen P, Velthaus JL, Rankin S, Clark RE, et al. Axl Blockade by BGB324 Inhibits BCR-ABL Tyrosine Kinase Inhibitor-Sensitive and -Resistant Chronic Myeloid Leukemia. *Clinical cancer research : an official journal of the American Association for Cancer Research.* 2017;23(9):2289-300.
44. Boshuizen J, Koopman LA, Krijgsman O, Shahrabi A, van den Heuvel EG, Ligtenberg MA, Vredevoogd DW, Kemper K, Kuilman T, Song JY, et al. Cooperative targeting of melanoma heterogeneity with an AXL antibody-drug conjugate and BRAF/MEK inhibitors. *Nat Med.* 2018;24(2):203-12.
45. Guo G, Gong K, Ali S, Ali N, Shallwani S, Hatanpaa KJ, Pan E, Mickey B, Burma S, Wang DH, et al. A TNF-JNK-Axl-ERK signaling axis mediates primary resistance to EGFR inhibition in glioblastoma. *Nat Neurosci.* 2017;20(8):1074-84.
46. Palisoul ML, Quinn JM, Schepers E, Hagemann IS, Guo L, Reger K, Hagemann AR, McCourt CK, Thaker PH, Powell MA, et al. Inhibition of the Receptor Tyrosine Kinase AXL Restores Paclitaxel Chemosensitivity in Uterine Serous Cancer. *Molecular cancer therapeutics.* 2017;16(12):2881-91.
47. Sen T, Tong P, Diao L, Li L, Fan Y, Hoff J, Heymach JV, Wang J, and Byers LA. Targeting AXL and mTOR Pathway Overcomes Primary and Acquired Resistance to WEE1 Inhibition in Small-Cell Lung Cancer. *Clinical cancer research : an official journal of the American Association for Cancer Research.* 2017;23(20):6239-53.
48. Brand TM, Hartmann S, Bhola NE, Li H, Zeng Y, O'Keefe RA, Ranall MV, Bandyopadhyay S, Soucheray M, Krogan NJ, et al. Cross-talk Signaling between HER3 and HPV16 E6 and E7 Mediates Resistance to PI3K Inhibitors in Head and Neck Cancer. *Cancer research.* 2018;78(9):2383-95.
49. Leonard B, Brand TM, O'Keefe RA, Lee ED, Zeng Y, Kemmer JD, Li H, Grandis JR, and Bhola NE. BET Inhibition Overcomes Receptor Tyrosine Kinase-Mediated Cetuximab Resistance in HNSCC. *Cancer research.* 2018;78(15):4331-43.
50. Li M, Lu J, Zhang F, Li H, Zhang B, Wu X, Tan Z, Zhang L, Gao G, Mu J, et al. Yes-associated protein 1 (YAP1) promotes human gallbladder tumor growth via activation of the AXL/MAPK pathway. *Cancer letters.* 2014;355(2):201-9.
51. Ghiso E, Migliore C, Ciciriello V, Morando E, Petrelli A, Corso S, De Luca E, Gatti G, Volante M, and Giordano S. YAP-Dependent AXL Overexpression Mediates Resistance to EGFR Inhibitors in NSCLC. *Neoplasia.* 2017;19(12):1012-21.

52. Boregowda RK, Medina DJ, Markert E, Bryan MA, Chen W, Chen S, Rabkin A, Vido MJ, Gunderson SI, Chekmareva M, et al. The transcription factor RUNX2 regulates receptor tyrosine kinase expression in melanoma. *Oncotarget.* 2016;7(20):29689-707.
53. Bae SY, Hong JY, Lee HJ, Park HJ, and Lee SK. Targeting the degradation of AXL receptor tyrosine kinase to overcome resistance in gefitinib-resistant non-small cell lung cancer. *Oncotarget.* 2015;6(12):10146-60.
54. Miller MA, Oudin MJ, Sullivan RJ, Wang SJ, Meyer AS, Im H, Frederick DT, Tadros J, Griffith LG, Lee H, et al. Reduced Proteolytic Shedding of Receptor Tyrosine Kinases Is a Post-Translational Mechanism of Kinase Inhibitor Resistance. *Cancer discovery.* 2016;6(4):382-99.
55. Yun MR, Lim SM, Kim SK, Choi HM, Pyo KH, Kim SK, Lee JM, Lee YW, Choi JW, Kim HR, et al. Enhancer Remodeling and MicroRNA Alterations Are Associated with Acquired Resistance to ALK Inhibitors. *Cancer research.* 2018;78(12):3350-62.
56. Scaltriti M, Elkabets M, and Baselga J. Molecular Pathways: AXL, a Membrane Receptor Mediator of Resistance to Therapy. *Clinical cancer research : an official journal of the American Association for Cancer Research.* 2016;22(6):1313-7.
57. Riesenberg S, Groetchen A, Siddaway R, Bald T, Reinhardt J, Smorra D, Kohlmeyer J, Renn M, Phung B, Aymans P, et al. MITF and c-Jun antagonism interconnects melanoma dedifferentiation with pro-inflammatory cytokine responsiveness and myeloid cell recruitment. *Nat Commun.* 2015;6(8755.
58. Usman MW, Gao J, Zheng T, Rui C, Li T, Bian X, Cheng H, Liu P, and Luo F. Macrophages confer resistance to PI3K inhibitor GDC-0941 in breast cancer through the activation of NF-kappaB signaling. *Cell death & disease.* 2018;9(8):809.
59. Britschgi A, Andraos R, Brinkhaus H, Klebba I, Romanet V, Muller U, Murakami M, Radimerski T, and Bentires-Alj M. JAK2/STAT5 inhibition circumvents resistance to PI3K/mTOR blockade: a rationale for cotargeting these pathways in metastatic breast cancer. *Cancer cell.* 2012;22(6):796-811.
60. Shrivastava S, Steele R, Sowadski M, Crawford SE, Varvares M, and Ray RB. Identification of molecular signature of head and neck cancer stem-like cells. *Sci Rep.* 2015;5(7819.
61. Bakiri L, Macho-Maschler S, Custic I, Niemiec J, Guio-Carrion A, Hasenfuss SC, Eger A, Muller M, Beug H, and Wagner EF. Fra-1/AP-1 induces EMT in mammary epithelial cells by modulating Zeb1/2 and TGFbeta expression. *Cell Death Differ.* 2015;22(2):336-50.
62. Dong C, Ye DX, Zhang WB, Pan HY, Zhang ZY, and Zhang L. Overexpression of c-fos promotes cell invasion and migration via CD44 pathway in oral squamous cell carcinoma. *J Oral Pathol Med.* 2015;44(5):353-60.
63. Zenz R, Scheuch H, Martin P, Frank C, Eferl R, Kenner L, Sibilia M, and Wagner EF. c-Jun regulates eyelid closure and skin tumor development through EGFR signaling. *Dev Cell.* 2003;4(6):879-89.
64. Fang Y, Wang Y, Wang Y, Meng Y, Zhu J, Jin H, Li J, Zhang D, Yu Y, Wu XR, et al. A new tumour suppression mechanism by p27Kip1: EGFR down-regulation mediated by JNK/c-Jun pathway inhibition. *Biochem J.* 2014;463(3):383-92.
65. Green MR, Rodig S, Juszczynski P, Ouyang J, Sinha P, O'Donnell E, Neuberg D, and Shipp MA. Constitutive AP-1 activity and EBV infection induce PD-L1 in Hodgkin lymphomas and posttransplant lymphoproliferative disorders: implications for targeted therapy. *Clinical cancer research : an official journal of the American Association for Cancer Research.* 2012;18(6):1611-8.
66. Skinner HD, Giri U, Yang LP, Kumar M, Liu Y, Story MD, Pickering CR, Byers LA, Williams MD, Wang J, et al. Integrative Analysis Identifies a Novel AXL-PI3 Kinase-PD-L1 Signaling Axis Associated with Radiation Resistance in Head and Neck Cancer. *Clinical cancer research : an official journal of the American Association for Cancer Research.* 2017;23(11):2713-22.
67. Aguilera TA, Rafat M, Castellini L, Shehade H, Kariolis MS, Hui AB, Stehr H, von Eyben R, Jiang D, Ellies LG, et al. Reprogramming the immunological microenvironment through radiation and targeting Axl. *Nat Commun.* 2016;7(13898.
68. Hart LS, Rader J, Raman P, Batra V, Russell MR, Tsang M, Gagliardi M, Chen L, Martinez D, Li Y, et al. Preclinical Therapeutic Synergy of MEK1/2 and CDK4/6 Inhibition in Neuroblastoma. *Clinical cancer research : an official journal of the American Association for Cancer Research.* 2017;23(7):1785-96.

Figure legends

Figure 1: AXL knockdown sensitizes HNSCC and ESCC cells to BYL719 in-vitro and in-vivo. **A.** Upper-panel analysis of BYL719 IC:50 values of in HPV^{Neg} and HPV^{Pos} cells following knockdown of AXL (shAXL1 and shAXL2), compared with control cells (shCT). Lower panel- WB analysis demonstrating AXL levels. **B.** WB analysis showing the AKT/mTOR pathway activation in $KYSE180^{Sen}$ cells, following AXL knockdown and BYL719 treatment (2μM, 24hr). **C.** Tumor growth of shCT or shAXL1 $KYSE180^{Sen}$ CDXs in mice treated daily with BYL719 25mg\kg. **D.** IHC analysis of the tumors showing the expression levels of the proliferation marker Ki67 and phosphorylated ribosomal S6 levels (pS6). A higher magnification is shown in the insert. **E.** Analysis of expression levels of IHC staining presented in D, using the 3DHISTECH software HistoQuant™.

Figure 2: The AP-1 transcriptional complex regulates AXL expression in HNSCC and ESCC. **A.** RNA sequencing data obtained from isogenic BYL719 sensitive vs. acquired resistance CAL33 and KYSE180 cells (HNSCC and ESCC, respectively). Presented in the Venn diagram are TFs signatures upregulated in BYL719 resistant cells, and their overlap with binding sites for TF in the promoter of AXL. **B.** WB analysis of CAL33 and KYSE180 BYL719-sensitive vs. resistant cells showing the expression of TF (l.e-long exposure. s.e-short exposure) **C.** A qPCR analysis comparing the mRNA levels of AXL and c-JUN in CAL33 and KYSE180 sensitive vs. resistant cells. **D.** IF images of CAL33 and KYSE180 BYL719-sensitive vs. resistant cells showing c-JUN (CY-3 labeled) in red, AXL (Alexa488 labeled) in green and DAPI in blue. **E.** Upper panel- WB analysis showing AXL levels following transfection with siRNA for the silencing of c-JUN and c-FOS. Lower panel- qPCR analysis showing AXL mRNA levels in cells transfected with siRNAs for the silencing of c-JUN and c-FOS. **F.** AXL receptor binding by c-JUN following chromatin immunoprecipitation in $KYSE180^{Sen}$ and $KYSE180^{Res}$ cells measured by qPCR.

Figure 3. AXL and c-JUN levels are correlated in clinical samples of HNSCC tumors, and cell lines. **A.** IHC analysis of AXL and c-JUN expression levels in a tissue array of HNSCC tumors. The brown and blue arrows highlights 2 different tumor samples, that correlate to the IHC images marked by the brown and blue rectangular in the left. AXL and c-JUN expression levels were calculated using the 3DHISTECH software HistoQuant™ **B.** WB analysis of AXL and c-JUN expression levels in patient tumor samples from Soroka Medical Center. A densitometry analysis of expression levels of AXL and c-JUN is presented in the graph. In left, IHC images of 2 of the patients demonstrating AXL and c-JUN expression in the tumor tissues. **C.** WB analysis of HPV^{Neg} and HPV^{Pos} HNSCC and ESCC cell lines, demonstrating the expression levels of AXL and c-JUN.

Quantification of the WB is presented in left, where each cell line in represented by a black (HPV^{Neg}) or blue (HPV^{Pos}) symbol, and the size of the symbol correlates to the BYL719 IC:50 value of the cell line in μM (i.e, the larger the symbol, the higher the IC:50. IC:50 values for HPV^{Neg} cells were extracted from our previous report (14)).

Figure 4: Silencing of c-JUN and c-FOS, or blocking c-JUN N-terminal Kinase (JNK) sensitizes HNSCC and ESCC cells to BYL719 in vitro. **A.** Analysis of BYL719 IC:50 values in HNSCC and ESCC cells following transfection with siRNAs to silence c-JUN and c-FOS expression. **B.** Analysis of BYL719 IC:50 values following JNK inhibition using SP600125 (5 and 10μM) in HNSCC and ESCC cells. **C.** WB analysis showing AXL level, and AKT/mTOR pathway activation in HNSSC and ESCC cells treated with BYL719 (2μM), SP600125 (5 and 10μM) and combination for 24hr. **D.** A qPCR analysis of AXL mRNA levels in cells treated as in with BYL719 (2μM), SP600125 (10μM) and combination for 24hr. **E.** Synergy test for the interaction between BYL719 and SP600125. The synergy test was analyzed using the Chalice software (Horizon), and a synergy score was extracted.

Figure 5: SP600125 enhances BYL719 efficacy in vivo in CDX and PDX models. **A-C**. Tumor growth of $KYSE180^{Sen}$ **(A)**, UTSCC47 **(B)** and HNSCC PDX-SE1 **(C)** following daily treatment with vehicle, BYL719 (25mg\kg), SP600125 (15mg\kg) and a combination. IHC staining of the tumors for the proliferation marker Ki67 is shown in left. The 3DHISTECH software HistoQuant™ was used analysis of IHC staining.

Figure 6: SP600125 increases BYL719 efficacy in vivo in syngeneic head and neck cancer models. **A.** IHC staining showing the expression of Ki67, pAKT, AXL, c-JUN and keratin-14 (KRT14) in 4NQO-induced tongue tumor region. **B**. Proliferation assay of 4NQO-induced tumor cell lines from the tongue and lips following 4 days treatments with BYL719 (2μM), SP600125 (5 and 10 μM) and combination. **C.** WB analysis of tongue and lips 4NQO-induced tumor cell lines following 24hr with the indicated treatments, showing the AKT/mTOR pathway activation. **D.** Survival rates of immunocompetent C57BL/6 mice in an orthotopic tongue cancer model following daily treatments with BYL719 (25mg\kg), SP600125 (15mg\kg) and a combination. T2 weighted coronal images of tongue lower panel show the difference in tumor progression following 10 days of treatments. **E.** Tumor growth of immunocompetent C57BL/6 mice baring a syngenic lips cancer model, treated as indicated in D.

Scheme 1: The proposed mechanism of AP-1/ AXL Driven Resistance to PI3Kαi in HNSCC and ESCC. Cells that aquire resistance to PI3Kαi upregulate AXL via the AP-1 transcription factors c-Jun and c-FOS. AXL dimerizes with EGFR and activates mTOR signaling in an AKT independent manner. Combination of the PI3Kα inhibitor BYL719 with the JNK inhibitor SP600125 sensitizes the cells to BYL719.

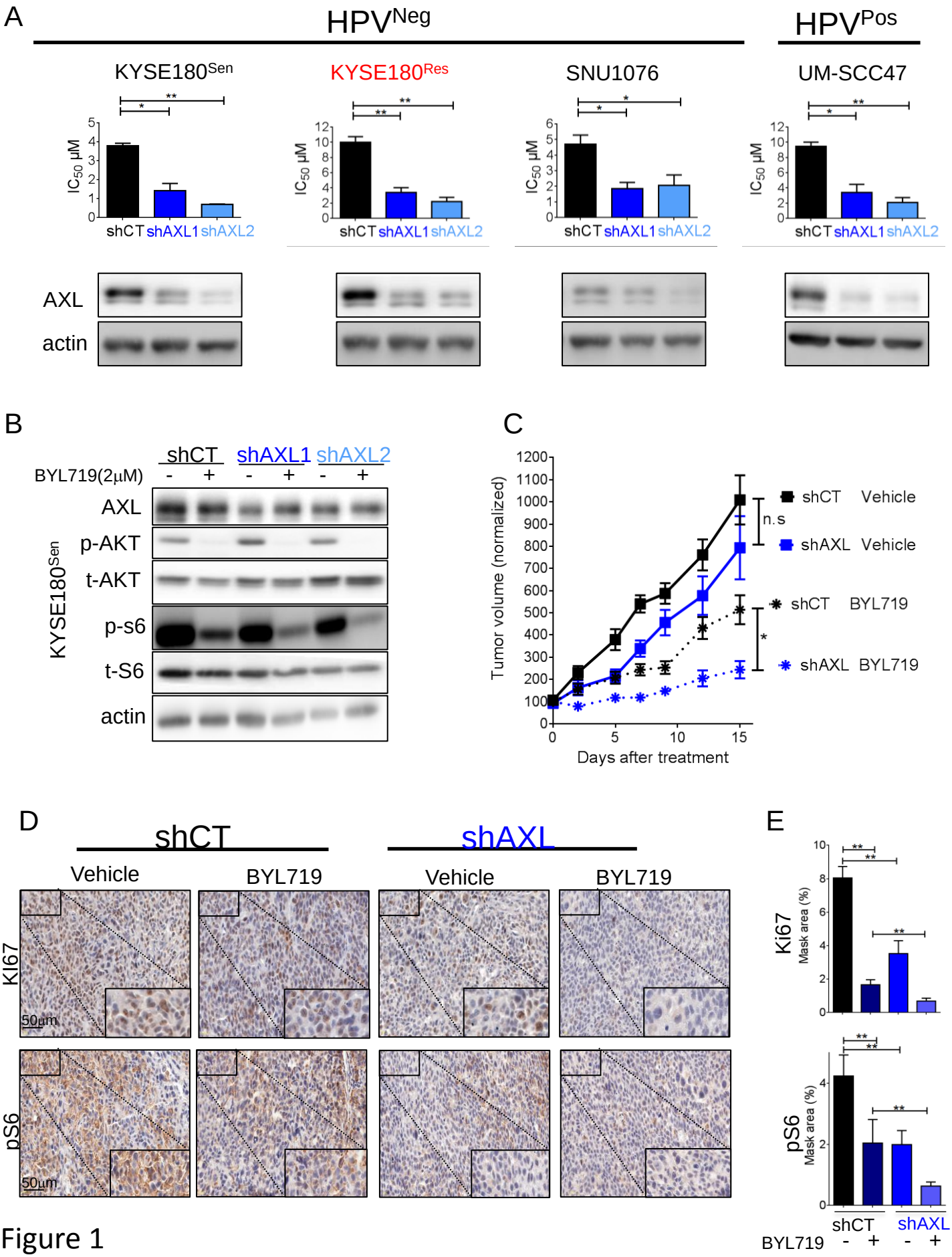
A
HPVNeg
HPVPos
KYSE180Sen
KYSE180Res
SNU1076
UM-SCC47
IC50 µM
shCT shAXL1 shAXL2
AXL
actin
B
shCT shAXL1 shAXL2
BYL719(2µM) - + - + - +
KYSE180Sen
AXL
p-AKT
t-AKT
p-s6
t-S6
actin
C
Tumor volume (normalized)
Days after treatment
shCT Vehicle
shAXL Vehicle
shCT BYL719
shAXL BYL719
n.s
D
shCT
shAXL
Vehicle
BYL719
Ki67
pS6
50µm
E
Ki67
pS6
Mask area (%)
shCT shAXL
BYL719 - + - +

Figure 1

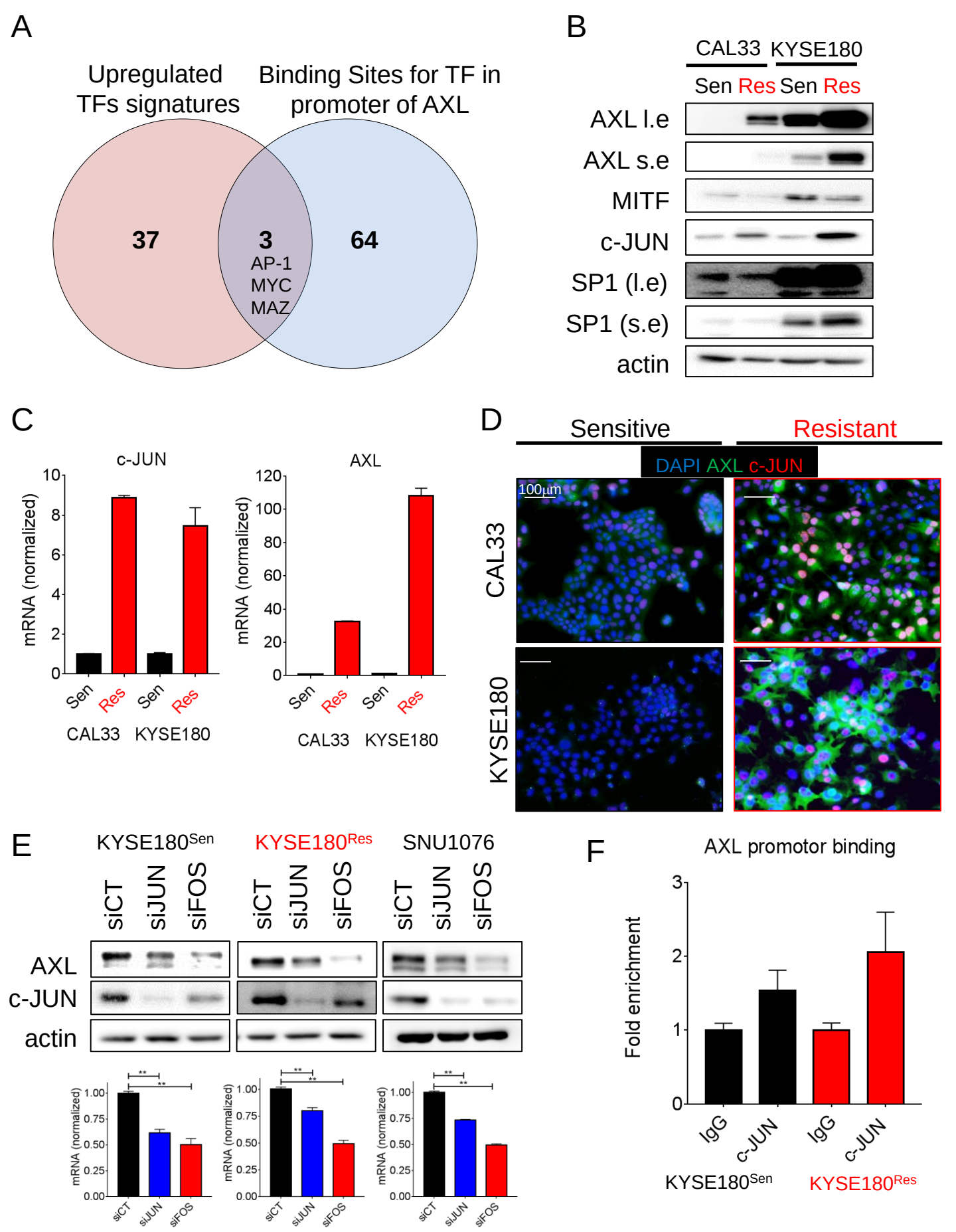
A
Upregulated TFs signatures
Binding Sites for TF in promoter of AXL
37
3
AP-1
MYC
MAZ
64
B
CAL33 KYSE180
Sen Res Sen Res
AXL l.e
AXL s.e
MITF
c-JUN
SP1 (l.e)
SP1 (s.e)
actin
C
c-JUN
AXL
mRNA (normalized)
Sen Res Sen Res
CAL33 KYSE180
D
Sensitive
Resistant
DAPI AXL c-JUN
100μm
CAL33
KYSE180
E
KYSE180Sen
KYSE180Res
SNU1076
siCT siJUN siFOS
AXL
c-JUN
actin
mRNA (normalized)
F
AXL promotor binding
Fold enrichment
IgG c-JUN IgG c-JUN
KYSE180Sen
KYSE180Res

Figure 2

A.

Tissue microarray

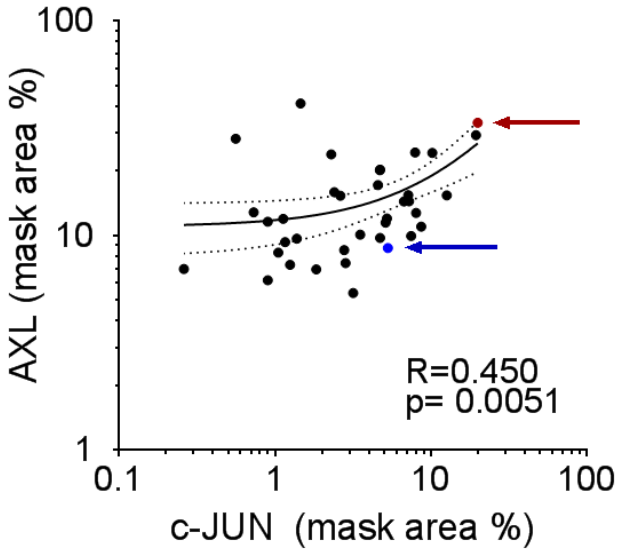

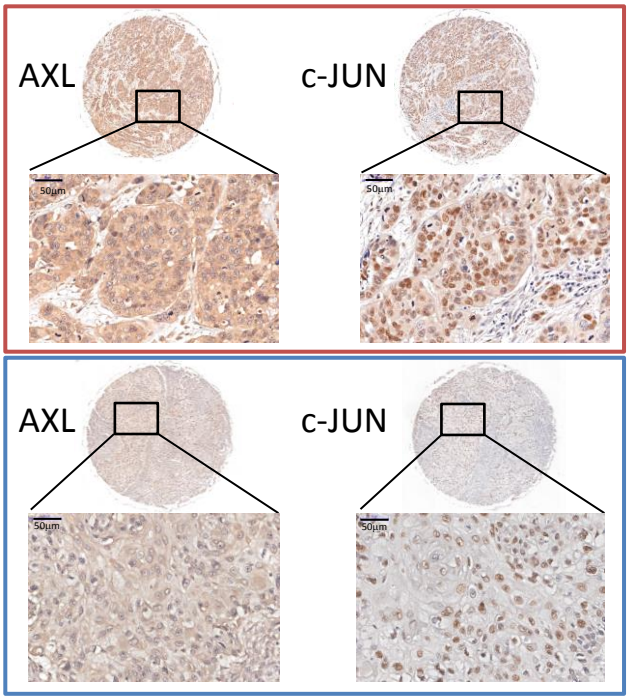

B.

Soroka's patients samples cohort

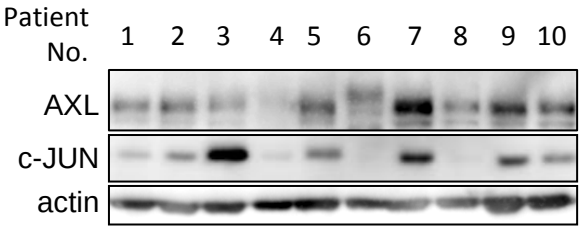

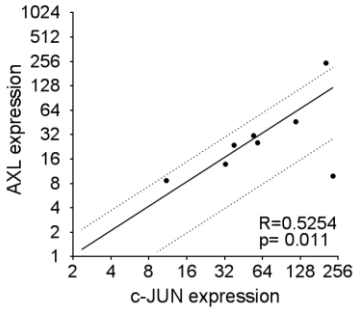

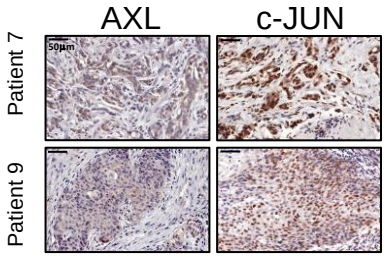

C.

Tumor cell lines

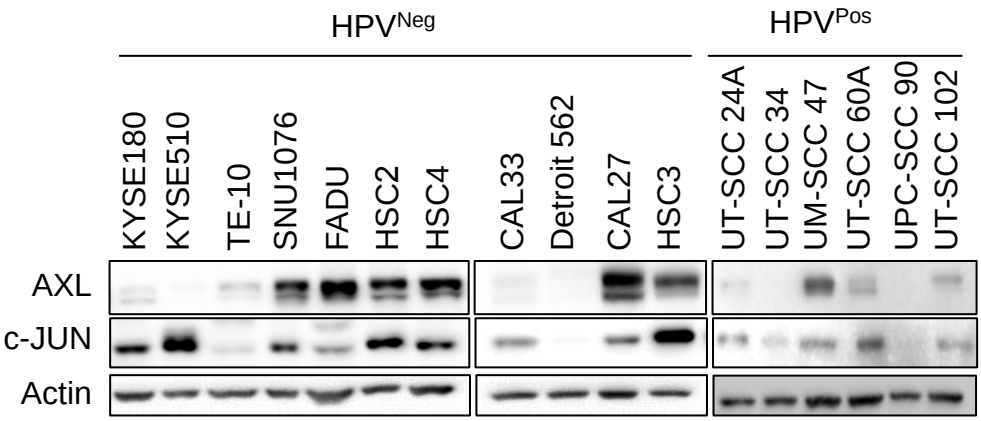

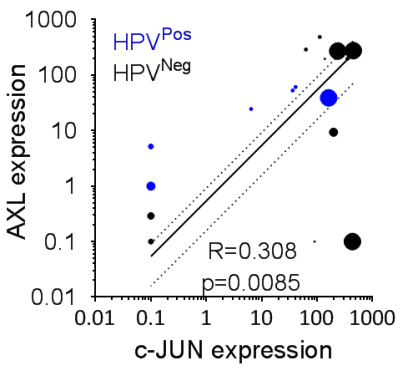

Figure 3

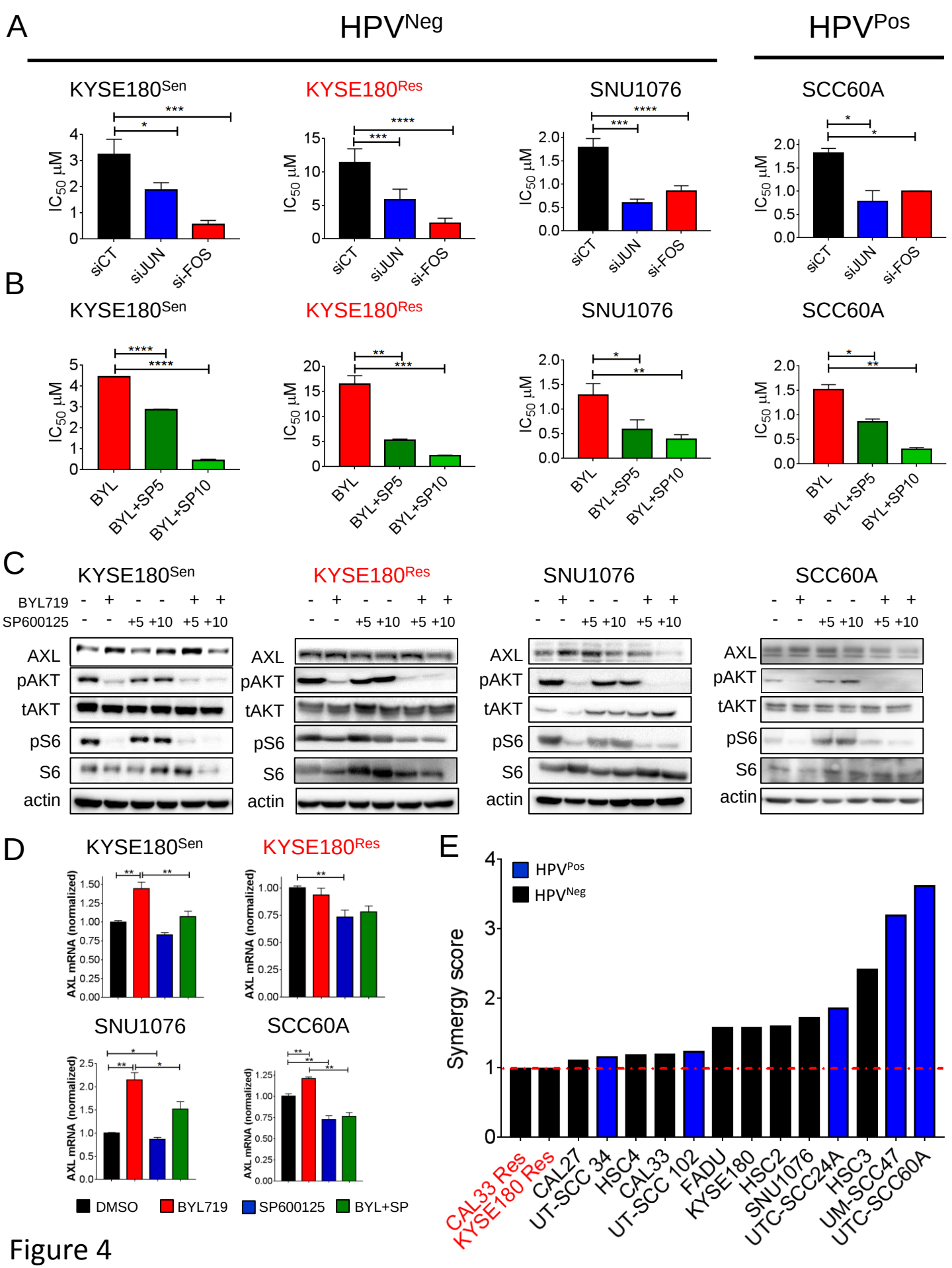
A
HPVNeg
HPVPos
KYSE180Sen
KYSE180Res
SNU1076
SCC60A
IC50 µM
siCT
siJUN
si-FOS
B
BYL
BYL+SP5
BYL+SP10
C
BYL719
SP600125
AXL
pAKT
tAKT
pS6
S6
actin
D
AXL mRNA (normalized)
DMSO
BYL719
SP600125
BYL+SP
E
HPVPos
HPVNeg
Symergy score
CAL33 Res
KYSE180 Res
CAL27
UT-SCC 34
HSC4
CAL33
UT-SCC 102
FADU
KYSE180
HSC2
SNU1076
UTC-SCC24A
HSC3
UM-SCC47
UTC-SCC60A

Figure 4

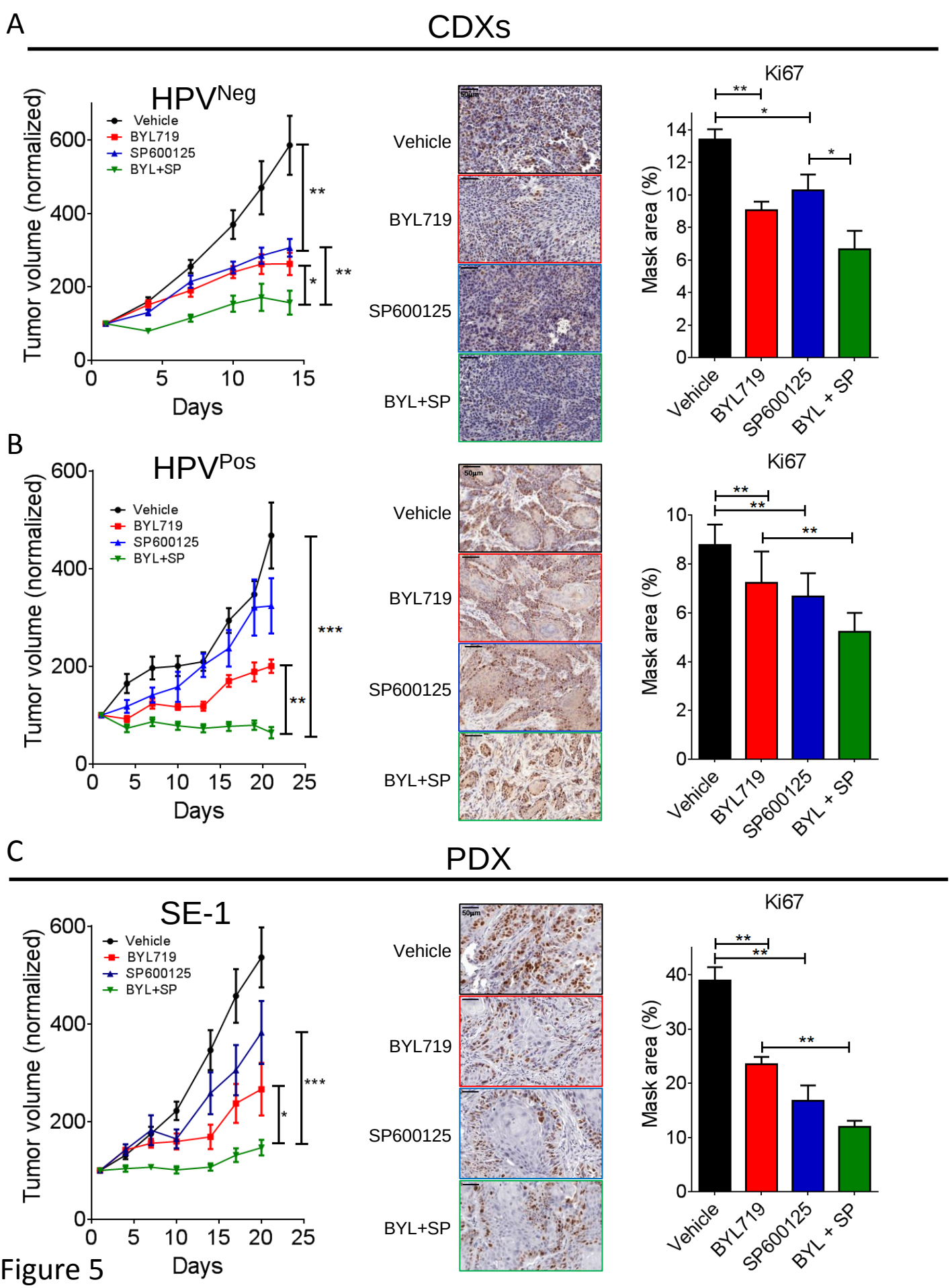
A
CDXs
HPVNeg
Vehicle
BYL719
SP600125
BYL+SP
Tumor volume (normalized)
Days
Vehicle
BYL719
SP600125
BYL+SP
Ki67
Mask area (%)
Vehicle
BYL719
SP600125
BYL + SP
B
HPVPos
Tumor volume (normalized)
Days
Vehicle
BYL719
SP600125
BYL+SP
Ki67
Mask area (%)
Vehicle
BYL719
SP600125
BYL + SP
C
PDX
SE-1
Tumor volume (normalized)
Days
Vehicle
BYL719
SP600125
BYL+SP
Ki67
Mask area (%)
Vehicle
BYL719
SP600125
BYL + SP

Figure 5

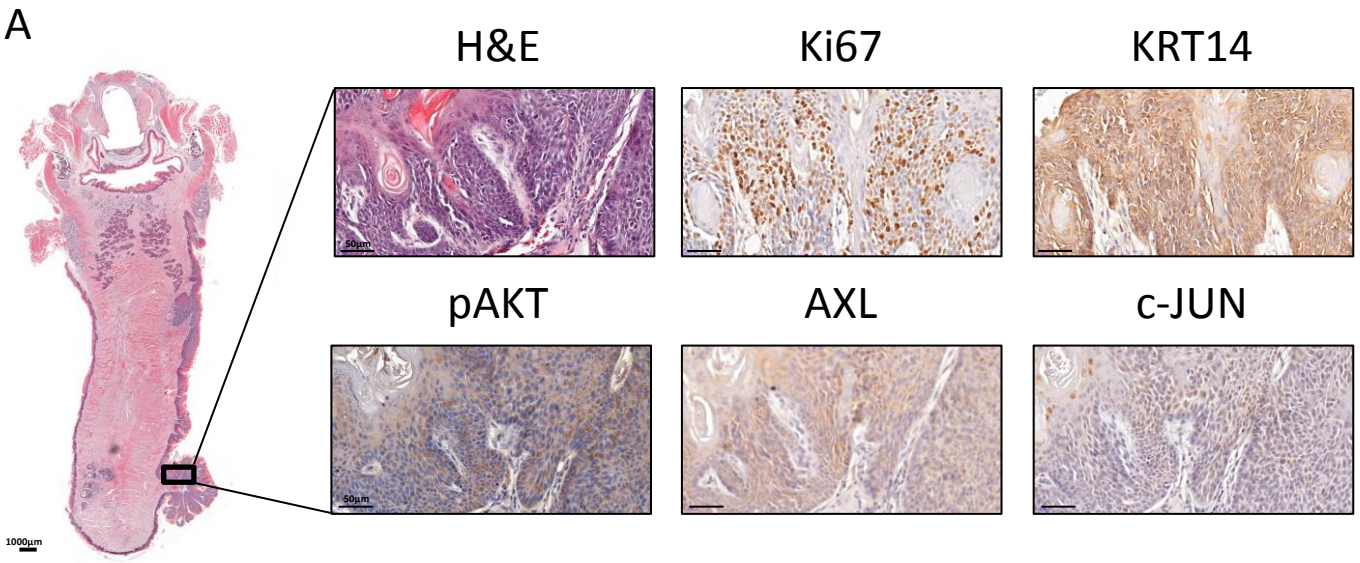
A
H&E
Ki67
KRT14
pAKT
AXL
c-JUN
1000µm
50µm

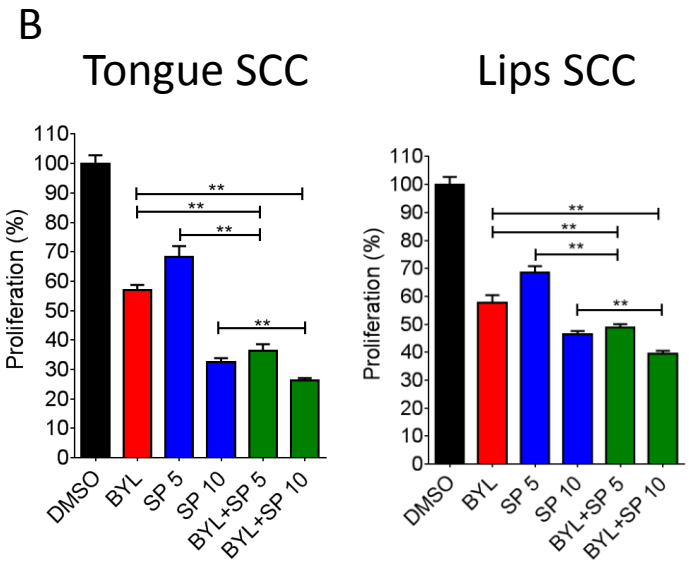
B
Tongue SCC
Lips SCC
Proliferation (%)
DMSO
BYL
SP 5
SP 10
BYL+SP 5
BYL+SP 10

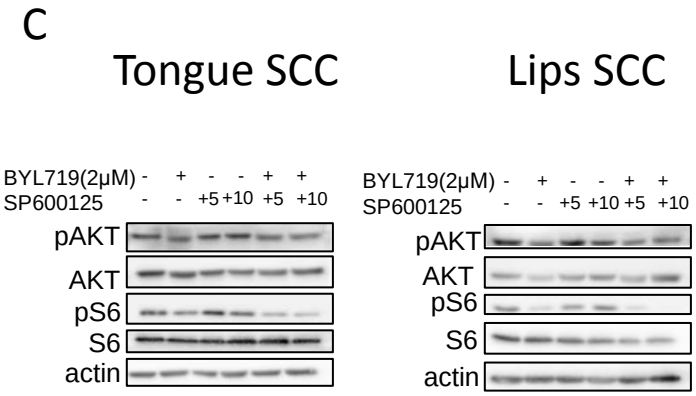
C
Tongue SCC
Lips SCC
BYL719(2µM)
SP600125
pAKT
AKT
pS6
S6
actin

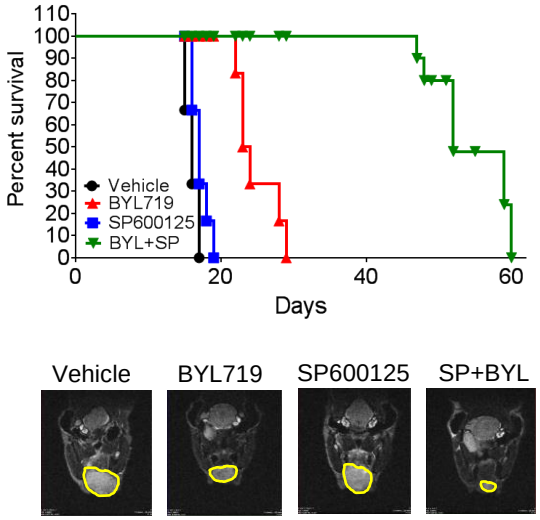
D
Percent survival
Days
Vehicle
BYL719
SP600125
BYL+SP

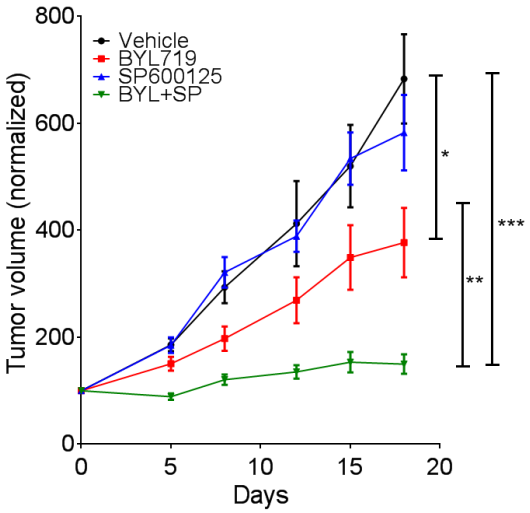
E
Tumor volume (normalized)
Days
Vehicle
BYL719
SP600125
BYL+SP

Figure 6

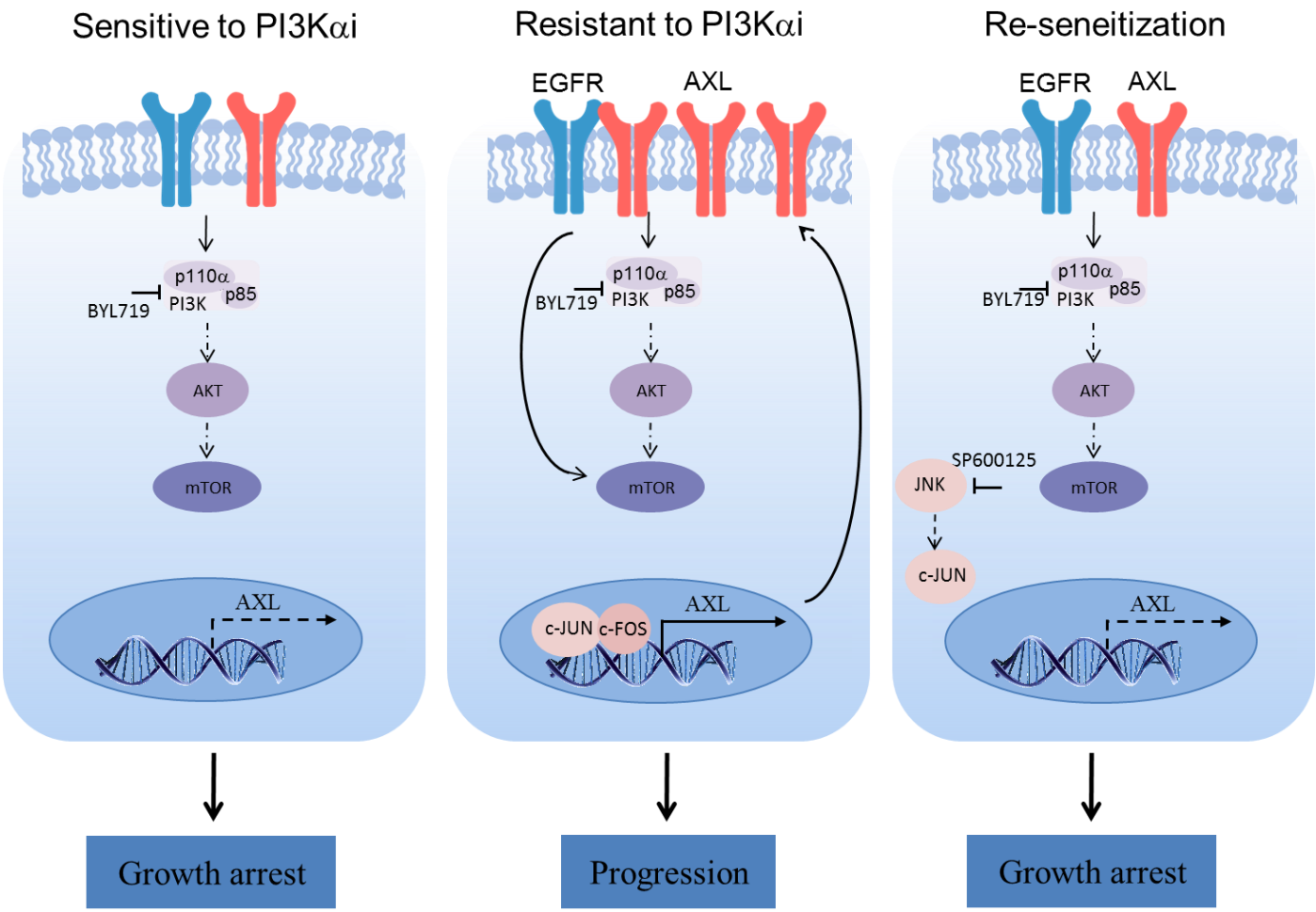
Sensitive to PI3Kαi
Resistant to PI3Kαi
Re-seneitization
EGFR
AXL
p110α
PI3K
p85
BYL719
AKT
mTOR
SP600125
JNK
c-JUN
c-FOS
AXL
Growth arrest
Progression
Growth arrest

Scheme 1